Published in final edited form as:
Small. 2010 August 16; 6(16): 1794–1805. doi:10.1002/smll.201000538.

Biocompatibility, Biodistribution, and Drug-Delivery Efficiency of Mesoporous Silica Nanoparticles for Cancer Therapy in Animals

Jie Lu,
California NanoSystems Institute, Department of Microbiology, Immunology and Molecular Genetics, University of California Los Angeles, 405 Hilgard Avenue, Los Angeles, California 90095 (USA)

Monty Liong,
California NanoSystems Institute, Department of Chemistry and Biochemistry, Jonsson Comprehensive Cancer Center, University of California Los Angeles, 405 Hilgard Avenue, Los Angeles, California 90095 (USA)

Zongxi Li,
California NanoSystems Institute, Department of Chemistry and Biochemistry, Jonsson Comprehensive Cancer Center, University of California Los Angeles, 405 Hilgard Avenue, Los Angeles, California 90095 (USA)

Jeffrey I. Zink, and
California NanoSystems Institute, Department of Chemistry and Biochemistry, Jonsson Comprehensive Cancer Center, University of California Los Angeles, 405 Hilgard Avenue, Los Angeles, California 90095 (USA)

Fuyuhiko Tamanoi
California NanoSystems Institute, Department of Microbiology, Immunology and Molecular Genetics, University of California Los Angeles, 405 Hilgard Avenue, Los Angeles, California 90095 (USA)

Fuyuhiko Tamanoi: fuyut@microbio.ucla.edu

Abstract

Mesoporous silica nanoparticles (MSNs) are a promising material for drug delivery. In this Full Paper, MSNs are first shown to be well tolerated, as demonstrated by serological, hematological, and histopathological examinations of blood samples and mouse tissues after MSN injection. Biodistribution studies using human cancer xenografts are carried out with in vivo imaging and fluorescent microscopy imaging, as well as with inductively coupled plasma mass spectroscopy. The results show that MSNs preferentially accumulate in tumors. Finally, the drug-delivery capability of MSNs is demonstrated by following tumor growth in mice treated with camptothecin-loaded MSNs. These results indicate that MSNs are biocompatible, preferentially accumulate in tumors, and effectively deliver drugs to the tumors and suppress tumor growth.

Keywords

animal model; biocompatibility; biodistribution; mesoporous silica nanoparticles; tumor suppression

Correspondence to: Jie Lu.

Supporting Information is available on the WWW under http://www.small-journal.com or from the author.

1. Introduction

The application of nanotechnology in the field of drug delivery has attracted much attention in recent decades.[1–7] Recent breakthroughs on the architectural control and surface functionalization of inorganic nanomaterial-based delivery vehicles, such as mesoporous silica nanoparticles (MSNs),[8–13] have brought new possibilities to this burgeoning area of research. The ability to functionalize the surface of these nanocarriers with stimuli-responsive groups for controlled release establishes them as a new platform for various biotechnological and biomedical applications.[1,4,6,14–21] Among a variety of inorganic-based nanomaterials, MSNs have several attractive features for application as a novel drug-delivery system, such as large surface areas, tailorable pore sizes, controllable particle sizes and shapes, and dual-functional surfaces (exterior and interior).[22] The size- and shape-controllable pores of MSNs can store pharmaceutical drugs and prevent their premature release and degradation before reaching their designated target. Chemotherapeutic drugs can be loaded to MSNs, replacing the need to use solvents that are often toxic for healthy tissues.[7,16]

We and other groups have already demonstrated that MSNs could be used as drug-delivery vehicles, gene-transfection reagents, cell markers, and carriers of molecules.[7,23–29] Conjugation with specific ligands or antibodies, such as folic acid, allows the targeting of nanoparticles to special cell types, such as cancer cells.[29] The ability to incorporate nanomachines in or outside the pores that respond to external stimuli, producing nanoimpeller- and nanovalve-equipped nanoparticles, opens unlimited possibilities of various controllable delivery systems.[6,20,30–33] In addition, the incorporation of superparamagnetic iron oxide nanocrystals in the core of mesoporous silica nanoparticles provides a promising reagent for biomedical imaging.[29,34] Therefore, MSNs are exciting and promising vehicles for various aspects of biomedical applications.

However, much research and investigation needs to be done and many questions remain to be answered before MSNs can be used as a drug-delivery system. Among these, a critical challenge is to have the capacity to deliver a sufficient amount of drug to a desired location with less acute or chronic toxicity than conventional therapies, such as chemotherapy. Our previous study, as well as results from other groups, suggested that at concentrations below 100 μg mL^{-1}, MSNs do not induce any cytotoxicity in a variety of cell lines.[7,13,16] Some growth inhibition was noted when the concentration exceeds 200 μg mL^{-1}. Our knowledge on the in vivo biocompatibility profile of MSNs is still very limited. Some recent studies reported that no severe toxicity to mice was observed when used in the short term at a concentration required for in vivo imaging.[35–37] Hudson et al.[38] reported that intraperitoneal or intravenous administration of 1.2 g kg^{-1} MSNs is lethal to SV129 mice but is safe when reduced to 40 mg kg^{-1}. These studies provide us with some preliminary insights into the toxicological profile of MSNs. However, a comprehensive and extensive investigation with practical dosages that are adequate and suitable for in vivo study is urgently needed for future clinical application.

The other important concern of MSNs is the lack of in vivo biodistribution information. It is important to understand where the MSNs distribute when injected into animals. One exciting reason for using nanoparticles as drug-delivery vehicles for cancer therapy is the enhanced permeability and retention (EPR) effect of macromolecules.[39,40] This theory postulates that certain sizes of particles tend to accumulate in tumor tissue much more than in normal tissues because a tumor's newly formed blood vessels are usually abnormal in form and architecture, poorly aligned with wide fenestrations, and lack a smooth muscle layer and tumors usually lack effective lymphatic drainage.[39,40] Based on this theory, it is expected

that MSNs with size of 100–130nm would be able to accumulate in a solid tumor and thus deliver a larger amount of chemotherapeutic drugs to tumors compared to normal tissues. The size of the MSNs we are using is ≈100–130 nm. To address these biodistribution issues, we decided to use human tumor xenografts in mice.

Another crucial question about MSNs concerns whether the success of using MSNs as a drug-delivery vehicle in vitro can be reproduced in in vivo animal study. Studies of the ability of MSNs to deliver different kinds of anticancer drugs in cultured cells have been reported but, surprisingly, our knowledge of the effect of MSNs in vivo is very limited at best. Although many publications have demonstrated encouraging results of using MSNs for in vitro cancer therapy, it is important to prove whether MSNs can indeed deliver and release the chemotherapeutic drugs to solid tumors in animals, either through the EPR effect or by positive targeting with tumor-specific ligands, before making any effort to further develop MSNs for clinical application.

In this Full Paper, we report our investigations on biocompatibility of MSNs and biodistribution in mice with established human cancer xenograft by using in vivo imaging, fluorescence microscopy, and mass spectrometry. We also test the ability of MSNs to deliver anticancer drugs into human xenograft in mice and to suppress the tumor growth.

2. Results

2.1. Characteristics of Fluorescent Mesoporous Silica Nanoparticles

Fluorescent mesoporous silica nanoparticles (FMSNs) were synthesized by sol–gel methods incorporating fluorescein isothiocyanate (FITC), as described previously and in the Experimental Section.[7,41] These nanoparticles were modified by addition of phosphonate. Electron microscopy and X-ray diffraction (XRD) analysis showed that the nanoparticles were roughly spherical in shape and ≈100–130 nm in diameter, with hexagonal arrays of pores (Figure 1A). An average pore diameter of ≈2 nm was observed by using transmission electron microscopy (TEM) and an interplanar spacing of $d(100)$ ≈4 nm was calculated from the XRD pattern. We have previously shown that these mesoporous silica nanoparticles can store anticancer drugs, such as camptothecin and taxol, and can deliver them to human cancer cells.[7,42] Both folic-acid-conjugated and nonconjugated FMSNs were used in this study and the characterization of folic-acid-conjugated FMSNs is described later in Section 2.4.

2.2. FMSNs are Well Tolerated in Mice

To determine the maximum tolerated dose of FMSNs, we injected intravenously (i.v.) female nude mice with various doses of FMSNs, ranging from 4 mg mouse^{-1} (≈200 mg kg^{-1}) to 0.25 mg mouse^{-1} (≈10 mg kg^{-1}), once per day for 10 d. All mice were healthy after 10 days of treatment but the mice treated with FMSNs higher than 2 mg mouse^{-1} (100 mg kg^{-1}) showed mild elevation of liver transaminase aspartate aminotransferase (AST) (see Supporting Information S1). Therefore, we decided that 1 mg mouse^{-1} (50 mg kg^{-1}) was the appropriate dose and was used for subsequent toxicity evaluations.

For acute and subacute toxicity profiling, 12 female nude mice were injected through the tail vein with FMSNs suspended in 0.1 mL saline solution with final concentrations of 0, 0.06, 0.12, 0.25, 0.5, and 1 mg mouse^{-1} d^{-1} (two mice for each dose), twice per week for 14 d (total of five doses). Approximately 60 μL of blood was collected from retroorbit at the 2nd day. Body-weight change, visible and/or palpable dermal infection, presence of ascites, and grooming or impaired mobility were closely monitored every day. A Body-condition scoring system was also used to evaluate the nutrition status of the mice. Compared with the control mouse, the body weights of all treated mice were similar, indicating a negligible acute

toxicity at even the highest dose (1 mg mouse^{-1} d^{-1}), as shown in Figure 1B. The body condition scores (BCS) of all mice were 3, which means well conditioned according to the published scale.[43] No infection, impaired mobility, or reduced food taking was observed. No obvious histological lesion with any of the tissues, neither gross nor pathological abnormality, was observed in major organs, such as the liver, spleen, kidney, heart, intestine, stomach, muscle, or lungs. Mild-to-moderate hepatic bile duct hyperplasia was found in all mice, which is a common and nonspecific occurrence in mice (Figure 1Bb and Table S2). Three mice treated with 0.5 mg mouse^{-1}, 0.12 mg mouse^{-1}, or 0.06 mg mouse^{-1} showed mild elevation of their neutrophil (NE) count at the 14th day (40.31, 50.57, and 55.99%, respectively; normal range: 6.6–38.9%; Table 1). One mouse treated with 0.5 mg mouse^{-1} showed a mildly elevated eosinophil count (4.12%; normal range: 0–3.9%) by the 14th day. The same mouse also showed a mildly elevated liver transaminase level (alanine aminotransferase (ALT), 296 U L^{-1}; AST, 450 U L^{-1}; normal range: 7–227 U L^{-1} for ALT, 37–329 U L^{-1} for AST).

To evaluate the relative long-term toxicity, two groups of mice (6 in each group) were administered with FMSNs at a dose of 1 mg mouse^{-1} d^{-1} or saline solution through intraperitoneal (i.p.) injection twice per week for 2 months (total injections: 18). Body-weight changes, dermal infection, the presence of ascites, and mobility were closely monitored every day. Throughout the study, no mouse exhibited unusual responses or behaviors (lethargy, weight-loss, immobility, etc.) compared to controls. Body-weight data are summarized in Figure 1Bc. Hematology results indicate that all measured factors were within normal ranges, suggesting that no inflammatory reaction was associated with the treatment. Two mice showed mildly elevated ALT and AST levels (Table S3). At the end of the experiment, no apparent histopathological abnormalities or lesions related to treatment were observed, with the exception of one mouse treated with FMSNs that showed mild, chronic, and multifocal gastritis. Representative histology results are shown in Figure 1Bd. All tested mice, including control mice, showed mild subacute splenomegaly, hepatomegaly, as well as bilateral renomegaly, based on percentage of body weight. The most probable diagnosis for these lesions is extramedullary hematopoiesis, since there was no evidence of lymphoid infiltration. The detailed histopathological report is provided in Table S3.

Since the mice injected with FMSNs showed little abnormality, we thought that FMSNs injected might be excreted from the animal body. To examine this, we measured Si concentrations in urine and feces collected from mice after injection of FMSN at different time points. The urine and feces collected by special metabolic cages for mice (as described in the Experimental Section) were analyzed with inductively coupled plasma optical emission spectrometry (ICP-OES), a method with a sensitivity in the low parts-per-billion (ng g^{-1}) range. A total of 1 mg of FMSN was injected into the mouse, which corresponds to ≈467 μg of Si. Within the first 24 h after injection, 122.8 μg of Si was detected in urine (26.3% of total). The renal excretions were decreasing with the following days (108.6 μg for the 2nd day, 61.7 μg for the 3rd day, and 49.6 μg for the 4th day). In contrast, in the feces, the excretions increase with the highest amount of Si being detected on the 4th day (9.1, 24.2, 27.4, and 37.2 μg for the 1st, 2nd, 3rd, and 4th days, respectively), although the amounts in feces are very small compared with urine. Figure 2 shows the cumulative amount of excreted Si for each day (48-h results show the sum of the amount of Si detected in the 1st and 2nd day). Within four days, almost all of Si injected into the mice bodies was excreted out through urine and feces (94.4% with 4 d). These results are quite interesting and might explain the low toxicity observed in the above biocompatibility experiments.

2.3. FMSNs Preferentially Accumulate in Tumors

To track the FMSNs in the mice bodies, we took advantage of the fluorescent dye, FTIC, that was incorporated into the nanoparticles when synthesized. This facilitated real-time

imaging of the in vivo biodistribution of FMSNs after systemic injection. The size of our FMSNs was ≈130 nm; as such, we expected that FMSNs would accumulate in tumors due to the EPR effect. In this study, we also examined folic-acid-conjugated FMSNs (F-FMSNs). Surface modification of the surface of the nanoparticles with folic acid, which specifically binds to folate receptor that is up-regulated in various types of human cancers, is expected to enhance tumor accumulation.

To establish human cancer xenografts, 5×10^6 human breast cancer cells, MCF-7, collected in 0.2 mL Dulbecco's modified eagle medium (DMEM), were subcutaneously (s.c.) injected into the left lateral abdominal wall of the nude mice. To promote growth of tumor, a sterilized 17β-estradiol pellet (17β-E2, 1.8 mg, 60-d release, produces 3–4 n_M E2 blood level; Innovative Research of America, FL) was implanted subcutaneously (s.c.) into the right side on the 33rd day. Mice were randomly divided into the treatment or vehicle groups in each experiment after tumors ≈3 mm in diameter were palpable.

The mice bearing subcutaneous tumors were injected via the tail vein with FMSNs or F-FMSNs suspended in saline solution. After 4, 24, or 48 h, the mice were anesthetized, placed in the chamber of a Maestro 2 in vivo imaging system, and optical light and green fluorescence images were obtained. As shown in Figure 3A, a very strong green fluorescence signal was detected in tumors of the mice treated with FMSNs at 4 and 24 h after the injection, indicating the accumulation of nanoparticles in tumors. After 48 h, the signal in the tumors decreased to the same level as the whole body. Similar results were obtained when F-FMSNs were injected.

After euthanasia, the tumor, liver, kidney, lung, heart, intestine, stomach, mesentery and spleen were collected and all tissues were analyzed by fluorescence imaging. For both FMSNs and F-FMSNs, the fluorescence signal from the tumors was much stronger than that from the other tissues at 4 and 24 h (Figure 3B). No significant differences were observed between FMSNs and F-FMSNs under microscope. The fluorescence intensity of the nanoparticles in tumors was weaker at 24 h than at 4 h but significantly stronger than that in other tissues. The next strongest fluorescence intensities were found in the kidney and liver. The localization of particles in the kidney is interesting and verifies previous work with surface-modified silica nanoparticles by He et al.[44]

Within liver, kidney and spleen, the nanoparticle fluorescence intensity peaked at 4 h, followed by a gradual decrease over 48 h. Close examination showed that the particles appeared to distribute into specific anatomic structures in these organs (Figure S2). They were highly condensed in the glomerulus and collecting ducts of the kidney at 4 h, then decreased afterwards. In the spleen, fluorescence was observed primarily in the red pulp, where red cells, macrophages, and phagocytes are abundant. In the liver, they were concentrated in the portal vein. In contrast, the particles were evenly distributed inside the cells as well as in the interstitial space of the tumors. Interestingly, a strong fluorescence signal was observed in the blood vessels of mice 4 h after injection and still observed 72 h after injection. The detection of green fluorescence in a smear of urine collected from bladder is consistent with the above ICP-experiment results, suggesting renal excretion.

2.4. Biodistribution Evaluations by ICP-MS

In order to obtain a quantitative measurement of the distribution of the nanoparticles, we used inductively coupled plasma mass spectroscopy (ICP-MS) to quantify the concentration of Si in each organ. As shown in Figure 4, 4 h after injection with FMSNs, the concentration of Si in tumor reached ≈45 ng mg^{-1} of tissue, while that in other organs ranged from 3 to 20 ng mg^{-1} of tissue. At 24 h after injection, the concentration in the tumor increased to≈110 ng mg^{-1}, while that in the kidney and lung increased to ≈40 ng mg^{-1} due to the abundant

blood supply. The accumulation of nanoparticles in other organs was reduced significantly to ≈3–10 ng mg^{-1}. At 48 h postinjection, while Si in other organs decreased further, the concentration of nanoparticles in tumors remained as high as 65 ng mg^{-1}. Compared to nontargeting nanoparticles, the folic-acid-modified particles F-FMSNs showed more-significant accumulation in tumors in comparison to other organs (Figure 4). The concentrations of Si in tumors were approximately 65, 170, and 90 ng mg^{-1} at 4, 24, and 48 h after injection, respectively, with the highest concentration observed at 24 h. In contrast, only 3–18 ng mg^{-1} of Si was detected in other organs within 48 h, including the kidney, spleen, intestine, liver, and heart. These results clearly demonstrated the preferential accumulation of silica nanoparticles in tumor xenograft of mice, probably due to the EPR effect, and folate-receptor-targeting conjugation further promoted this tumor-preferential accumulation of particles.

2.5. In vitro Effects of Drug-Loaded FMSNs

The above observations that our nanoparticles accumulate in subcutaneous xenograft encouraged us to examine the efficacy of these nanoparticles in delivering anticancer drugs. Before the in vivo study, we examined the effect of nanoparticles delivering camptothecin (CPT) in human cancer cell lines. In our previous study,[7,29] we successfully delivered CPT into human pancreatic cancer cells, PANC-1, inducing apoptosis. Elevated accumulation of particles in cells expressing a folate receptor and more cell-death-inducing effects with F-FMSNs than nontargeting FMSNs were observed. In the present study, we tested the effects on human breast cancer cells, SK-BR-3 and MCF-7, and a breast fibroblast, MCF10F.

By using UV/Vis absorption spectroscopy, only a minimal amount of drug molecules were observed in the supernatant when the CPT-loaded nanoparticles were dispersed in aqueous solution, even after thorough sonication and being suspended for 6 h, suggesting the stable loading of drug molecules in the pores of particles (data not shown). Based on UV/Vis absorption measurements, the amount of drug molecules that were stored in the core–shell nanoparticles was ≈29 nmol CPT in 1 mg of nanoparticles.

For specific cancer-targeted drug delivery, the intracellular integration and drug-delivery efficiency of F-FMSNs were compared to those of FMSNs. The effect of folic acid conjugation on the cellular uptake of nanoparticles was examined with a breast cancer cell, SK-BR-3, and a normal breast cell, MCF10F. Enhanced expression of folate receptor was detected in SK-BR-3 cells but not in MCF10F cells (Figure 5B), as reported previously.[45] Although the cellular internalization of FMSNs was observed in both cell lines, the amount of internalized F-FMSNs in SK-BR-3 was increased significantly compared to FMSNs, while no obvious change was seen in MCF10F, by both fluorescence microscopy and flow cytometry analysis (Figure 5C). These results corroborated the up-regulated folate-receptor expression on SK-BR-3, which may facilitate the recognition of the folic-acid-conjugated MSNs and enhance the uptake through folate-receptor-mediated endocytosis. Therefore, the ability of nanoparticles delivering chemotherapeutic drugs into cells was examined by measuring cytotoxicity induced by the drug, CPT, loaded in the pores of both nanoparticles. As shown in Figure 5D, both FMSN and F-FMSNs loaded with CPT induced cytotoxicity, suggesting that nanoparticles are capable of delivering hydrophobic chemicals into cells and exert cell-killing effects, consistent with our previous observations.[7] However, there was a considerable increase in the antitumor activity of folate-conjugated CPT-loaded F-FMSNs to SK-BR-3 cells, which correlated with the aforementioned enhanced particle uptake. More importantly, the cytotoxicity between the F-FMSNs and CPT-loaded FMSNs was similar for MCF10F cells since expression of the receptors on these cells are not up-regulated. The result suggested that the conjugation of folate to the nanoparticle facilitated the targeting to

folate-receptor-positive tumor cells, which naturally leads us to investigate the effect of these cancer-targeting particles in animal xenograft models.

2.6. In vivo Tumor-Suppressing Effect of Drug-Loaded FMSNs

Thirty nude mice with established xenografts of human breast cancer cell MCF-7 were randomly divided into 5 groups and intraperitoneal injections were started when the average tumor diameter reached 3 mm (14^{th} day after inoculation, see Supporting Information). Animals in the first group received saline solution as a control. Group 2 was treated with camptothecin dissolved in dimethyl sulfoxide (DMSO) and diluted in saline. Group 3 was treated with plain FMSNs without loading. Group 4 was treated with FMSNs loaded with CPT (the final concentration of CPT is the same as group 2). Group 5 was treated with F-FMSNs loaded with CPT. All injections were performed twice per week until the end of the experiment (the 68^{th} day). Each mouse was injected 18 times in total. The average body weights are shown in Figure 6A. Only one mouse in group 2 exhibited severe toxicity at the 45^{th} day, manifested by shivering, inactivity, severe necrosis of the tail, ataxic gait, and sudden drop of body weight (≈16.3 g). 50 mg mL^{-1} Amoxicillin (amoxil drop, Pfizer Inc) was administered in the drinking water but no improvement was observed after 3 d. This mouse was therefore euthanized on the 51^{st} day.

As shown in Figure 6B, the tumors in the control group (group 1) and FMSN-treated group (group 3) kept growing, showing a fast growing period after the inoculation of the 17β-estradiol pellet on the 31^{st} day. No significant difference in average tumor volumes was observed between these two groups, suggesting that FMSNs themselves did not affect the tumor growth in mice. Inhibition of tumor growth was significant in the CPT-treated group (group 2). At the end of this experiment (the 68^{th} day), administration of CPT suppressed the tumors to ≈14% of control, suggesting that it is an effective tumor-suppressing agent when dissolved in DMSO. However, from day 48, the average tumor volumes in groups treated with CPT-loaded FMSN or CPT-loaded F-FMSN (group 4 and 5) continuously declined, showing faster tumor-shrinking effects. No obvious subcutaneous tumors were visible on the 62nd day (Figure 6B and C).

The results of the histopathological examination of the mice's organs and the hematology and serology examinations are summarized in Table S3. Mild subacute splenomegaly, hepatomegaly, bilateral renomegaly, and cardiomegaly, based on percentage of body weight, were observed in all surviving mice, which are common and nonspecific findings in nude mice. Mild-to-moderate lymphoid hyperplasia and moderate chronic bilateral adrenal capsular fibrosis were also detected in all mice except the control mice. In addition, mildly elevated hematocrite was also seen in all mice. The blood test from mice of group 2 (CPT-treated mice) showed moderately to severely elevated liver enzymes (ALT, AST), moderate-to-severe hypoalbuminemia and hypoproteinemia, mildly elevated creatinine kinase as well as mildly to moderately decreased levels of calcium and phosphorus. Group 3 (treated with FMSN alone) only showed mildly elevated ALT and AST. In groups 4 and 5 (treated with FMSN-loaded CPT and F-FMSN-loaded CPT, respectively), severely or mildly to moderately elevated liver enzymes (ALT, AST) were detected.

3. Discussion

We first report that FMSNs are well tolerated when injected in mice. In our present study, with treatment for 14 d, only one mouse treated with 50 mg kg^{-1} showed a mildly elevated eosinophil count and mildly elevated liver transaminase level. In the two-month study, no apparent histopathological abnormalities or lesions related to these animals treated with MSNs were observed, with the exception of one mouse showing mild gastritis and two mice with mildly elevated liver aminotransferases. These mild changes can easily result from

stress or exercise and thus do not necessarily indicate toxicity. In our acute toxicity study, pulmonary venous thrombus was observed in one mouse. However, this observed thrombus was not associated with any pathology and was neither organized nor covered by endothelium. Our data suggest that this dosage (50 mg kg^{-1}), which is demonstrated by previous in vitro studies and the present in vivo study, is adequate for pharmacological application for cancer therapy. On the other hand, Hudson et al.[38] reported that 30 mg $mouse^{-1}$ (≈1.5 g kg^{-1}) of intraperitoneally injected mesoporous silicate nanoparticles resulted in death or distress necessitating euthanasia. The toxicity observed by Husdon et al. [38] might be due to the extremely high dosage used (≈1.5 g kg^{-1}) and different size and composition. The biocompatibility of MSNs may depend on the materials' size, morphology, composition, and surface chemistry in addition to the dosage used.[46] For instance, Blumen et al. reported that surface modification, such as PEGylation (where PEG refers to poly(ethylene glycol)), produced mesoporous silicates that were nontoxic in peripheral tissue,[47] suggesting that coating strategies may systemically reduce toxicity. Also, experiments using MSNs as bioimaging vehicles in vivo with varying dosages (100 and 200 mg kg^{-1}) did not reveal any toxic effects.[35–37]

With the fluorescence tracking for distribution experiments, a quick and dense accumulation of nanoparticles in tumors was observed. For both FMSNs and F-FMSNs, a strong fluorescence signal was observed in the tumor compared to other tissues. The localization of particles in the kidney confirms renal excretion of MSNs, in agreement with our findings and other published studies.[44–48] Long retention of MSNs in blood circulation was observed. To further investigate the biodistribution of MSNs, we next used ICP-MS to examine the amount of silica. Preferential accumulation of FMSNs and F-FMSNs in the tumor was confirmed. A different time course of MSN accumulation in tumor was observed between the two methods. The fluorescence of FITC reached peak at 4 h, while the peak concentration of Si was found at 24 h. The reason for this difference is unclear at the moment. The fluorescence self-quenching character of FITC might be partly responsible for this phenomenon due to the complicated interaction with proteins in animal bodies.[49]

As for the significance of cancer-cell-targeting with folate, our results with ICP-MS showed slightly enhanced accumulation in tumors than that with nontargeting nanoparticles. However, both the fluorescence and ICP-MS studies point to significant amounts of FMSNs accumulated in the tumor. This is likely due to the EPR effect, that is, leaky vasculature of blood vessels in the tumor. Since our nanoparticles have average diameters of 100–130 nm, they may preferentially leak out from blood vessels.

An interesting observation we made concerns the rapid excretion of MSNs from animal bodies. In our present study, we observed that ≈95% of Si was excreted out of body through urine and feces, suggesting a quick and complete clearance of nanoparticles by the animal body. This is consistent with the reports of He et al. and Burns et al. that renal clearance was the major route of excretion.[44,48] He et al.[44] found that MSNs with sizes of ≈45 nm accumulated mainly in the liver, kidney, and urinary bladder a few hours after intravenous injection and silica nanoparticles are safely excreted through the renal route. Burns et al.[48] reported that silica-based nanoparticles with smaller sizes (3.3 and 6.0 nm) are found in circulating blood even after 48 h, with minimal retention in the major organs, and the renal filtration was the major route of excretion. These published data are consistent with our observations, although the authors used different MSNs with different sizes and surface modification and no human cancer xenograph was examined.

The most critical question regarding the use of MSNs for cancer therapy is its actual efficacy for delivering anticancer drugs to real tumors and suppressing their growth. Although many studies have demonstrated that MSNs are very promising candidate materials for drug

delivery for cancer therapy, to the best of our knowledge, no investigation has been reported so far proving this possibility in vivo. In the present study, we demonstrate, for the first time, that MSNs are very effective for antitumor drug delivery and that the tumor suppression is significant. The tumors in the mice treated with CPT-loaded FMSNs or CPT-loaded F-FMSNs were virtually eliminated at the end of experiments. These results proved that the high drug-loading ability, low toxicity, and tumor-accumulating effect of MSNs provide a promising drug-delivery vehicle for anticancer drugs. The tumor-curing results here are encouraging, building the basis for further investigation of the capacity of MSNs for other types of tumors and the possibility of using lower dosage to further reduce toxicity. Conjugation with folic acid on the surface showed a slight but not significant increase in the tumor-suppressing effect. This is unexpected, since we observed increased cell killing in the in vitro study and greater accumulation in tumors with F-FMSNs in animals, as detected by ICP-MS. Two possibilities may explain these results. First, the high dosages and large number of injections may suppress the tumors very quickly, thereby masking the enhanced effect of using F-FMSNs. Second, the expression of folate receptor on MCF-7 was not up-regulated as highly as on SK-BR-3, only relatively enhanced,[45] therefore, the specific binding between F-FMSNs and MCF-7 cells might not be strong enough to manifest a significant difference in tumor-suppressing ability in animals. These possibilities are currently evaluated with various dosages and frequency and with other human cancer cell lines in a future study.

4. Conclusions

Together, our findings showed that FMSNs are biocompatible at the effective dosages, capable of reducing toxicity of anticancer drugs, accumulate in tumor xenografts with or without targeting, are excreted quickly, effectively deliver anticancer drug to tumors, and exhibit excellent tumor-suppressing effect. These properties can be utilized to improve the efficiency of anticancer drugs through increased accumulation in tumors. These provide us with the confidence for further exploring mesoporous silica nanoparticles as promising novel vehicles for cancer therapy.

5. Experimental Section

Synthesis of mesoporous silica nanoparticles

FMSNs were synthesized by first dissolving FITC (5.5 mg) in absolute ethanol (3 mL) before adding aminopropyltriethoxysilane (APTS; 12 μL). In another container, cetyltrimethylammonium bromide (CTAB; 0.5 g) was dissolved in a solution of distilled water (240 mL) and sodium hydroxide (2 M, 1.75 mL) that was heated to 80 °C and stirred vigorously. The FITC/APTS solution was stirred under an inert atmosphere for 2 h before adding tetraethylorthosilicate (TEOS; 2.5 mL). Once the temperature of the CTAB solution had stabilized, the ethanol solution containing TEOS and FITC/APTS was added. After 15 min, 0.63 mL 3-trihydroxysilylpropyl methylphosphonate was slowly added to the mixture. After 2 h, the solution was cooled to room temperature and the particles were filtered and washed with methanol using a fritted funnel. The particles were allowed to dry at room temperature overnight. To remove the surfactants from the pores of the particles, particles (850 mg) were dissolved in a solution of methanol (90 mL) and hydrochloric acid (12.1 M, 5 mL) and refluxed for 24 h. The particles were then filtered and washed thoroughly to remove the surfactants and unbound FITC.

Synthesis of folic-acid-conjugated FMSNs and drug loading

To attach folic acid to FMSNs, 20 mg of particles were washed with and resuspended in DMSO. In a flask, folic acid (0.1 mg, Sigma, 98%) and APTS (0.05 μL) were mixed in

DMSO (1 mL). *N*-hydroxysuccinimide (0.03 mg, Aldrich, 98%) and 1-(3-dimethylaminopropyl)-3-ethylcarbodiimide hydrochloride (0.05 mg, Alfa Aesar, 98%) was then added into the mixture and stirred for 2 h. In a separate flask containing toluene (4 mL) and the FMSNs–DMSO suspension, the folate/APTS solution was added and the mixture was stirred for 20 h at room temperature. The materials were recovered by centrifugation, washed twice with toluene, and dried under vacuum. To load camptothecin (CPT; Sigma, 95%), 10 mg of the particles were suspended in a solution of drugs (1 mg) and DMSO (0.25 mL) for 4 h. After centrifuging the drug-loaded FMSNs from the suspension and removing the supernatant completely, the materials were dried under vacuum. The drug-loaded FMSNs were then washed and sonicated with water before being resuspended in aqueous solution. In order to determine the amount of drugs inside the FMSNs, the aqueous drug-loaded FMSN suspension was incubated at 4 °C for 6 h before centrifugation to show that the drugs were not being slowly released from the mesopores. The resulting supernatant was mixed with the previous supernatant solution from the washing process and measured by UV/Vis absorption spectroscopy. The pellet of drug-loaded FMSNs was resuspended and sonicated in DMSO and collected by centrifugation. The process was repeated two more times (≈15 min, total time) to ensure that the drugs were completely removed from the pores. The DMSO (or methanol) supernatants were then measured using UV/Vis absorption.

Cells and culture

The human breast cancer cell lines, MCF-7, MCF10F, and SK-BR-3, obtained from American Type Culture Collection, were maintained in DMEM supplemented with fetal calf serum (10%, Sigma, MO), L-glutamine (2%), penicillin (1%), and streptomycin (1%). The medium was routinely changed every 3 d and the cells were separated by trypsinization before reaching confluency.

Animals

All animal experiments were performed following the protocols approved by the UCLA Animal Research Committee. Six-week-old female BALB/cAnNCrj-nu nude mice (purchased from Charles River Laboratories) were maintained in disposable plastic cages with hardwood chips bedding in an air-conditioned room with a 12-h-light–12-h-dark cycle and given food (oriental CRF-1) irradiated with 30 Gy rays and filtered tap water ad libitum.

Human cancer xenograph establishment

5×10^6 human breast cancer cells, MCF-7, collected in DMEM (0.2 mL), were s.c. injected into the left lateral abdominal wall of the nude mice. To promote the tumorigenesis, a sterilized 17β-estradiol pellet (17β-E2, 1.8 mg, 60-d release, produces 3–4 n_M E2 blood level; Innovative Research of America, FL) was implanted subcutaneously into the left side on the 33rd day. Mice were randomly divided into treatment or vehicle groups in each experiment after tumors of ≈3 mm in diameter were palpable.

Biodistribution of FMSNs in animals with human xenograft

Different methods were used to determine the distribution of FMSNs in the mouse body. The green fluorescence of the nanoparticles at an excitation wavelength of 470 nm was used to track the nanoparticles using a Maestro 2 in vivo imaging system (CRi, MA) and a fluorescence microscope (Imager Z1, Leica) was used to detect the nanoparticles in the animals. For quantification, the Si concentration in each organ of the mice was determined by ICP-MS (Varian Inc.). Briefly, the nude mice bearing subcutaneous tumors were injected via the tail vein with FMSNs suspended in saline solution. The mice were anesthetized with isoflurane 4, 24 or 48 h later, put into the chamber of Maestro 2 in vivo imaging system, and the optical light and green fluorescence images were acquired for analysis. After the in vivo

imaging, all mice were euthanized by CO_2 and all organs were collected, including the subcutaneous tumors. Half of the tissues were embedded, frozen, processed to 4-μm slides by our tissue-processing core lab (TPCL, UCLA). One slide from each tissue sample was stained with hematoxylin and eosin. All slides were then analyzed under the fluorescence microscope. The other tissues were weighed and digested by heating in 1:1:1 H_2O/HF/HNO_3 mixture and analyzed by ICP-MS. The concentrations of Si in each organ were converted to units of nanograms per mg of organ.

Measurement of MSN excretion in urine and feces with ICP-OES

To measure the excretion of MSN from urine and feces, special single-mouse metabolic cages (Tecniplast) were used. Three nude mice were housed in the metabolic cages. 1 mg of FMSNs was i.p. injected into the mice. Urine and feces were collected into separate collection tubes before and after the injections at different time points. The collected urine and feces were sent to the molecular instrumentation center at UCLA for ICP analysis of Si.

Cell-death assay

The cytotoxicity assay was performed using a cell-counting kit (Dojindo Molecular Technologies, Inc). Briefly, cancer cells were seeded in 96-well plates (5000 cells $well^{-1}$) and incubated in fresh culture medium at 37 °C in a 5% CO_2/95% air atmosphere for 24 h. The cells were then washed with phosphate-buffered saline (PBS) and the medium was changed to a fresh medium with indicated MSNs or MSN loaded with chemicals at indicated concentrations. After the indicated incubation period, the cells were washed again with PBS and then 10% WST-8 solution in DMEM (100 μL) was added to the wells, which were then incubated for a further 2 h. The optical density (OD) was measured at 450 nm with a plate reader. Since the absorbance is proportional to the number of viable cells in the medium, the viable cell number was determined using a previously prepared calibration curve (Dojindo Co.).

Flow cytometry analysis

Flow cytometry analysis was used to detect the fluorescence signal of nanoparticles internalized by human cells. Briefly, the cells treated with FMSNs or F-FMSNS for 4 h were collected, washed with PBS, and analyzed with a fluorescence-activated cell sorter (Caliber, Becton Dickinson).

Tumor-growth assay

Thirty nude mice with the above-mentioned established xenograft of MCF-7 were randomly divided into 6 groups. Animals in group 1 received injection of saline solution (0.2 mL, 0.9%) through intraperitoneal. Animals in group 2 received i.p. injection of CPT (0.2 mL, 7.8 μM, dissolved in DMSO, and then diluted in saline to achieve the final concentration; the final concentration of DMSO was <1.5%). Animals in group 3 received i.p. injection of FMSNs (0.2 mL, 5 mg mL^{-1}). Animals in group 4 received i.p. injection of FMSNs loaded with CPT (0.2 mL, 5 mg mL^{-1}, the final concentration of CPT was ≈7.8 μ_M). Animals in group 5 received i.p. injection of folic-acid-conjugated FMSNs loaded with CPT (0.2 mL, 5 mg mL^{-1}). All injections were done twice per week from the right lower corner of the abdomen until the end of the experiment. The tumor volume and body weight were monitored every other day and the tumor volume was calculated using the following formula: tumor volume=$4\pi/3 \cdot LW^2/8$ where L is the length and W is the width of the tumor. On the final day, all mice were sacrificed and subjected to autopsy. Blood was collected for serological and hematological examination and organs for histopathological examination by a pathologist.

Supplementary Material

Refer to Web version on PubMed Central for supplementary material.

Acknowledgments

We thank Dr. Luis Papa and Dr. Gregory W. Lawson at the Division of Laboratory Animal Medicine of UCLA for help with the processing and analysis of the tissue sections, Dr. Matthew J. Schibler at the Macro-Scale Imaging Core Facility of California NanoSystems Institute of UCLA for help with the Maestro 2 in vivo imaging system, Dr. Shane Que Hee at the ICP-MS facility of UCLA for analysis of the Si concentration in animal tissues, and Dr. Armando Durazo at the UCLA Molecular Instrumentation Center for analysis of Si in urine and feces with ICP-OES. This work was supported by NIH grants CA133697 and CA41996, NSF-CHE-0809384, US DOD (HDTRA1-08-1-0041), and the UC Lead Campus for Nanotoxicology Training and Research, funded by UC TSR&TP, and a grant from Nanopacific Holdings Inc.

References

1. Zhao Y, Trewyn BG, Slowing II, Lin VS. J. Am. Chem. Soc. 2009; 131:8398–8400. [PubMed: 19476380]
2. Singh R, Lillard JWJ. Exp. Mol. Pathol. 2009; 86:215–223. [PubMed: 19186176]
3. Patil YB, Swaminathan SK, Sadhukha T, Ma L, Panyam J. Biomaterials. 2009; 31:358–365. [PubMed: 19800114]
4. Klichko Y, Liong M, Choi E, Angelos S, Nel AE, Stoddart JF, Tamanoi F, Zink JI. J. Am. Ceram. Soc. 2009; 92:s2–s10. [PubMed: 19834571]
5. Murakami T, Tsuchida K. Mini. Rev. Med. Chem. 2008; 8:175–183. [PubMed: 18289101]
6. Lu J, Choi E, Tamanoi F, Zink JI. Small. 2008; 4:421–426. [PubMed: 18383576]
7. Lu J, Liong M, Zink JI, Tamanoi F. Small. 2007; 3:1341–1346. [PubMed: 17566138]
8. Xia T, Kovochich M, Liong M, Meng H, Kabehie S, George S, Zink JI, Nel AE. ACS Nano. 2009; 3:3273–3286. [PubMed: 19739605]
9. Cauda V, Schlossbauer A, Kecht J, Zurner A, Bein T. J. Am. Chem. Soc. 2009; 131:11361–11370. [PubMed: 19722649]
10. Shylesh S, Wagner A, Seifert A, Ernst S, Thiel WR. Chemistry. 2009; 15:7052–7062. [PubMed: 19569138]
11. Chung TH, Wu SH, Yao M, Lu CW, Lin YS, Hung Y, Mou CY, Chen YC, Huang DM. Biomaterials. 2007; 28:2959–2966. [PubMed: 17397919]
12. Han YF, Chen F, Zhong Z, Ramesh K, Chen L, Widjaja E. J. Phys. Chem. B. 2006; 110:24450–24456. [PubMed: 17134200]
13. Slowing I, Trewyn BG, Lin VS. J. Am. Chem. Soc. 2006; 128:14792–14793. [PubMed: 17105274]
14. Mortera R, Vivero-Escoto J, Slowing II, Garrone E, Onida B, Lin VS. Chem. Commun. 2009:3219–3221.
15. Trewyn BG, Giri S, Slowing II, Lin VS. Chem. Commun. 2007:3236–3245.
16. Lai CY, Trewyn BG, Jeftinija DM, Jeftinija K, Xu S, Jeftinija S, Lin VS. J. Am. Chem. Soc. 2003; 125:4451–4459. [PubMed: 12683815]
17. Hom C, Lu J, Tamanoi F. J. Mater. Chem. 2009; 19:6308–6316. [PubMed: 20740060]
18. Nguyen TD, Leung KC, Liong M, Pentecost CD, Stoddart JF, Zink JI. Org. Lett. 2006; 8:3363–3366. [PubMed: 16836406]
19. Patel K, Angelos S, Dichtel WR, Coskun A, Yang YW, Zink JI, Stoddart JF. J. Am. Chem. Soc. 2008; 130:2382–2383. [PubMed: 18232687]
20. Ferris DP, Zhao YL, Khashab NM, Khatib HA, Stoddart JF, Zink JI. J. Am. Chem. Soc. 2009; 131:1686–1688. [PubMed: 19159224]
21. Angelos S, Yang YW, Patel K, Stoddart JF, Zink JI. Angew. Chem. Int. Ed. 2008; 47:2222–2226.
22. Kobler J, Moller K, Bein T. ACS Nano. 2008; 2:791–799. [PubMed: 19206612]
23. Radu DR, Lai CY, Jeftinija K, Rowe EW, Jeftinija S, Lin VS. J. Am. Chem. Soc. 2004; 126:13216–13217. [PubMed: 15479063]

24. Jin S, Leach JC, Ye K. Methods Mol. Biol. 2009; 544:547–557. [PubMed: 19488722]
25. Slowing II, Vivero-Escoto JL, Wu CW, Lin VS. Adv. Drug. Deliv. Rev. 2008; 60:1278–1288. [PubMed: 18514969]
26. Torney F, Trewyn BG, Lin VS, Wang K. Nat. Nanotechnol. 2007; 2:295–300. [PubMed: 18654287]
27. Santra S, Liesenfeld B, Dutta D, Chatel D, Batich CD, Tan W, Moudgil BM, Mericle RA. J. Nanosci. Nanotechnol. 2005; 5:899–904. [PubMed: 16060150]
28. Bottini M, Cerignoli F, Mills DM, D'Annibale F, Leone M, Rosato N, Magrini A, Pellecchia M, Bergamaschi A, Mustelin T. J. Am. Chem. Soc. 2007; 129:7814–7823. [PubMed: 17542582]
29. Liong M, Lu J, Kovochich M, Xia T, Ruehm SG, Nel AE, Tamanoi F, Zink JI. ACS Nano. 2008; 2:889–896. [PubMed: 19206485]
30. Du L, Liao S, Khatib HA, Stoddart JF, Zink JI. J. Am. Chem. Soc. 2009; 131:15136–15142. [PubMed: 19799420]
31. Angelos S, Khashab NM, Yang YW, Trabolsi A, Khatib HA, Stoddart JF, Zink JI. J. Am. Chem. Soc. 2009; 131:12912–12914. [PubMed: 19705840]
32. Khashab NM, Belowich ME, Trabolsi A, Friedman DC, Valente C, Lau Y, Khatib HA, Zink JI, Stoddart JF. Chem. Commun. 2009:5371–5373.
33. Coti KK, Belowich ME, Liong M, Ambrogio MW, Lau YA, Khatib HA, Zink JI, Khashab NM, Stoddart JF. Nanoscale. 2009; 1:16–39. [PubMed: 20644858]
34. Jang JT, Nah H, Lee JH, Moon SH, Kim MG, Cheon J. Angew. Chem. Int. Ed. 2009; 48:1234–1238.
35. Liu HM, Wu SH, Lu CW, Yao M, Hsiao JK, Hung Y, Lin YS, Mou CY, Yang CS, Huang DM, Chen YC. Small. 2008; 4:619–626. [PubMed: 18491363]
36. Hsiao JK, Tsai CP, Chung TH, Hung Y, Yao M, Liu HM, Mou CY, Yang CS, Chen YC, Huang DM. Small. 2008; 4:1445–1452. [PubMed: 18680095]
37. Kim J, Kim HS, Lee N, Kim T, Kim H, Yu T, Song IC, Moon WK, Hyeon T. Angew. Chem. Int. Ed. 2008; 47:8438–8441.
38. Hudson SP, Padera RF, Langer R, Kohane DS. Biomaterials. 2008; 29:4045–4055. [PubMed: 18675454]
39. Matsumura Y, Maeda H. Cancer Res. 1986; 46:6387–6392. [PubMed: 2946403]
40. Muggia FM. Clin. Cancer Res. 1999; 5:7–8. [PubMed: 9918196]
41. Huh S, Wiench JW, Yoo JC, Pruski M, Lin VSY. Chem. Mater. 2003; 15:4247–4256.
42. Lu J, Liong M, Sherman S, Xia T, Kovochich M, Nel AE, Zink JI, Tamanoi F. Nanobiotechnology. 2007; 3:89–95. [PubMed: 19936038]
43. Ullman-Cullere MH, Foltz CJ. Lab. Anim. Sci. 1999; 49:319–323. [PubMed: 10403450]
44. He X, Nie H, Wang K, Tan W, Wu X, Zhang P. Anal. Chem. 2008; 80:9597–9603. [PubMed: 19007246]
45. Jhaveri MS, Rait AS, Chung K-N, Trepel JB, Chang EH. Mol. Cancer Ther. 2004; 3:1505–1512. [PubMed: 15634643]
46. Hussain SM, Braydich-Stolle LK, Schrand AM, Murdock RC, Yu KO, Mattie DM, Schlager JJ, Terrones M. Adv. Mater. 2009; 21:1549–1559.
47. Blumen SR, Cheng K, Ramos-Nino ME, Taatjes DJ, Weiss DJ, Landry CC, Mossman BT. Am. J. Respir. Cell Mol. Biol. 2007; 36:333–342. [PubMed: 17038662]
48. Burns AA, Vider J, Ow H, Herz E, Penate-Medina O, Baumgart M, Larson SM, Wiesner U, Bradbury M. Nano Lett. 2008; 9:442–448. [PubMed: 19099455]
49. Deka C, Lehnert BE, Lehnert NM, Jones GM, Sklar LA, Steinkamp JA. Cytometry. 1996; 25:271–279. [PubMed: 8914824]

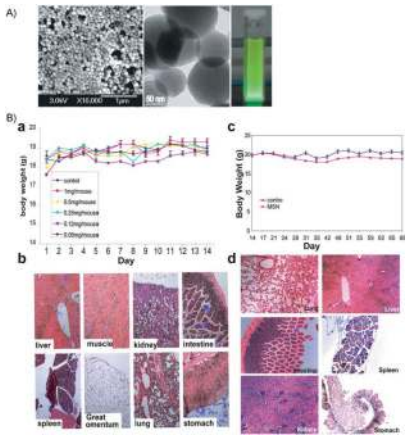

Figure 1.

A) Characterization of FMSNs. Left: scanning electron microscopy image of FMSNs; middle: transmission electron microscopy images of FMSNs; right: bright-green photoluminescence observed from porous silicon nanoparticles under UV/Vis light. B) Toxicity evaluation of FMSNs. 12 female mice i.v. injected with indicated doses of FMSNs (two mice for each dose), twice per week for 14 d (total of five doses): a) Average body weights. The results are presented as mean values ± the standard deviation (SD). b) Representative tissue sections of mice stained with hematoxylin and eosin. Long-term toxicity evaluation of FMSNs in mice. Two groups of mice (n = 6) were administered with FMSNs at a dose of 1 mg mouse^{-1} day^{-1} (50 mg kg^{-1}) (MSN group) or saline solution (control group) through i.p. twice per week for 2 months (total injections: 18). c) Average body weights of mice shown as mean values ± SD. d) Representative tissue sections of mice stained with hematoxylin and eosin are shown.

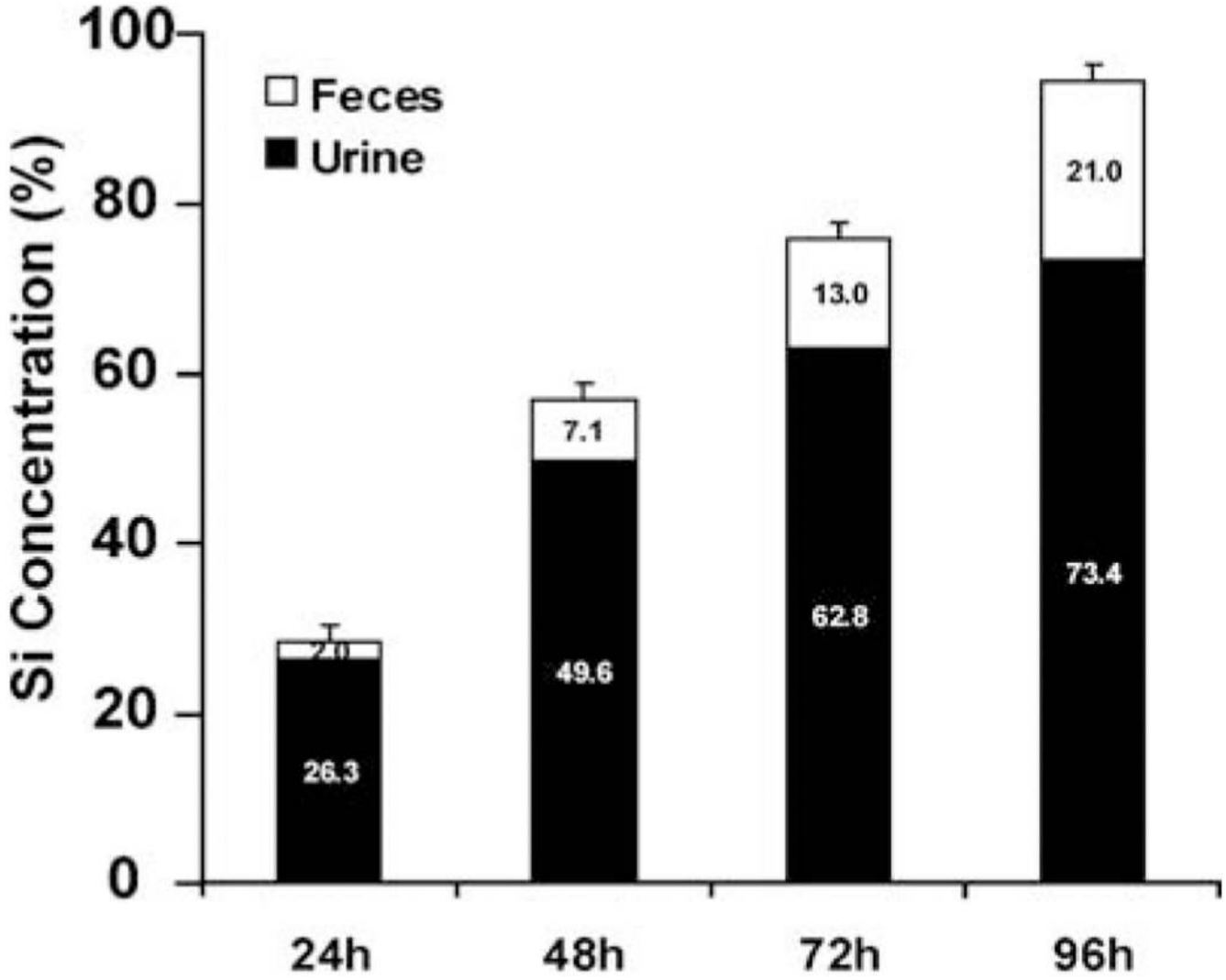

Figure 2.
ICP-OES analysis of the Si concentration in urine and feces of mice collected after injection of FMSN. The numbers shown are the average percentages of Si detected in urine and feces compared to the total injection amount of FMSN (1 mg).

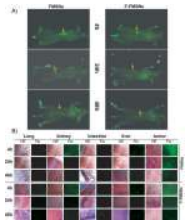

Figure 3.

Biodistribution of FMSNs in mice with xenograft tumors. Nude mice bearing subcutaneous human breast tumors were injected via the tail vein with FMSNs or F-FMSNs. 4, 24 or 48 h later, the mice were anesthetized and subjected to a Maestro 2 in vivo imaging system for green fluorescence images. The mice organs and tumors were then collected, cut into 4-μm sections, and analyzed with fluorescence microscopy. The times shown here indicate the times after injection of MSNs. A) Representative fluorescence images of mice taken with a Maestro 2 in vivo imaging system. The yellow arrows show the subcutaneous tumors. B) Representative tissue sections of mice are shown. All images shown here are 100× magnification. HE = hematoxylin and eosin stain; Flu = fluorescence images taken with fluorescence microscope.

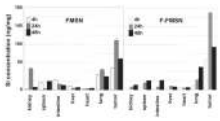

Figure 4.
ICP-MS quantitative measurement of Si concentrations in each organ of the mice with xenograft tumors. The mice bearing subcutaneous human breast tumors were injected with FMSNs or F-FMSNs. Mice organs were collected and Si concentrations were measured with ICP-MS. The average Si concentrations of each organ of the mice are shown as nanogram of Si per milligram of tissue. The results are shown as mean values ± SD.

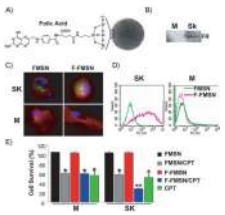

Figure 5.

The effect of folic acid conjugation with MSNs. A) Schematic illustration of FMSNs modified with folic-acid-targeting ligands on the surface. B) Western blot analysis shows that the folate receptor (FR) is up-regulated in breast cancer cell line Sk-BR-3 but not in MCF10F. M = MCF10F; SK = SK-BR-3. C) Fluorescence microscopy images show the internalization of FMSNs and F-FMSNs in SK-BR-3 (SK) and MCF10F (M) cells. The cell nuclei were stained with Hoechst 33342 (blue). Plasma membranes were stained with fluorescent wheat germ agglutinin (Molecular Probes). The green fluorescence indicates MSNs. Increased cellular internalization of F-FMSNs was observed in SK-BR-3 cells. D) Flow cytometry analysis results. The green fluorescence signals were collected in SK-BR-3 (SK) and MCF10F (M) cells after 4 h of treatment with either FMSNs or F-FMSNS. The right shift of the peak of the FL1-H channel indicates increased intracellular fluorescence. E) Cell-proliferation assay with FMSNs and F-FMSNs in MCF10F (M) and SK-BR-3 (SK) cells. The cells were treated for 48 h with 20 μg mL^{-1} of nanoparticles only (FMSN), CPT-loaded nanoparticles (FMSN/CPT), CPT-loaded F-FMSNs, or the same concentration of CPT dissolved in DMSO. The cells were then washed and stained with 10% WST-8 solution from the cell-counting kit (Dojindo Co.) for 2 h. The absorbances were measured at 450 nm with a plate reader. The percentages of each sample relative to control cells are presented as mean values ± SD.

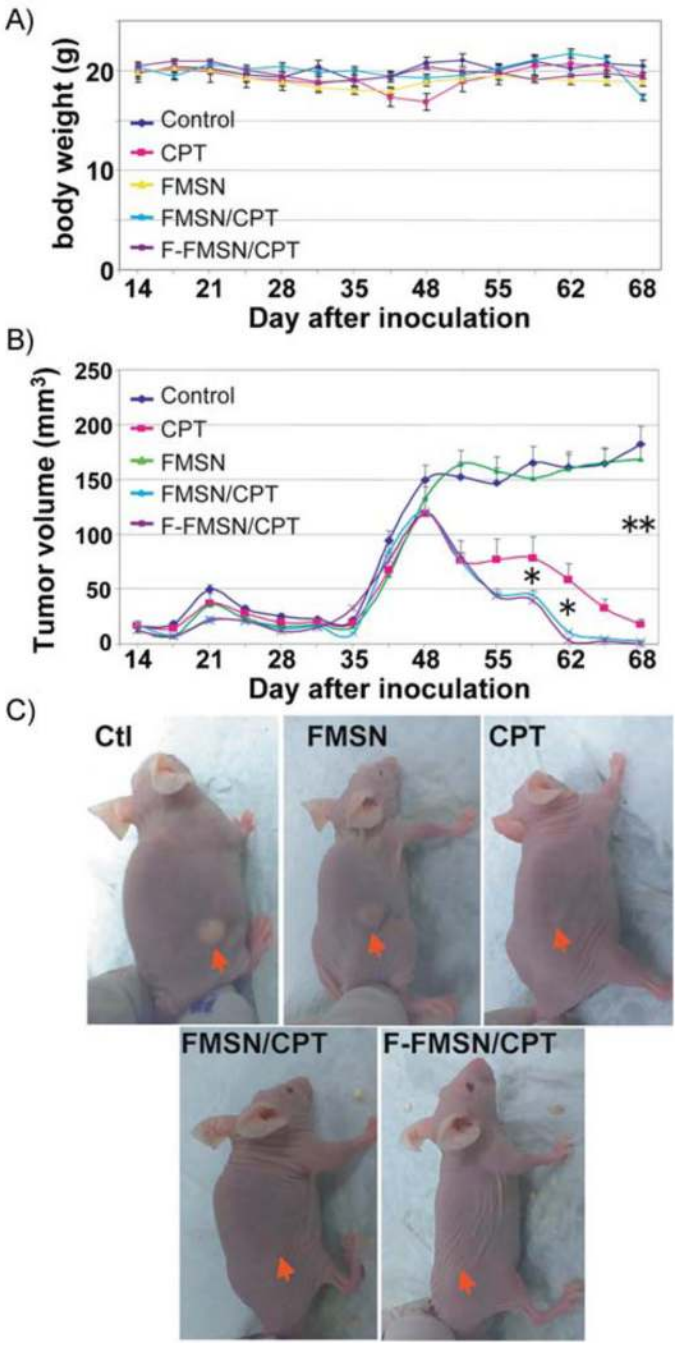

Figure 6.

Antitumor effects of mesoporous silica nanoparticles loaded with CPT in mice. Thirty nude mice with xenografts of human breast cancer cell MCF-7 were divided into 5 groups ($n = 6$) and intraperitoneal injections were started from the 14th day after inoculation. Animals were injected with either saline solution as a control, CPT, FMSNs without loading (FMSN), FMSNs loaded with CPT (FMSN/CPT), or F-FMSNs loaded with CPT (F-FMSN/CPT) twice per week until the end of the experiment (the 68th day). A) Average body weights shown as means ± SD. One mouse in the CPT-treated group was euthanized on the 51st day due to manifestation of severe toxicity. B) The average tumor volumes are shown as means

± SD. * = $p < 0.05$; ** = $p < 0.01$. C) Representative images of mice from different groups. Red arrows indicate the location of subcutaneous tumors.

Table 1

Serological and hematological results of mice treated with MSNs for 14 d.

	Normal range	Control	Treated mice [mouse^{-1}]				
		0	1 mg	0.5 mg	0.25 mg	0.1 mg	0.05 mg
CBC							
WBC [K μL^{-1}]	1.8–10.7	2.36	2.82	4.34		2.6	1.74
NE	6.6–38.9%	34.36	38.49	40.31*		50.75*	55.99*
LY	55.8–91.6%	59.90	54.25	45.53		42.12	34.94
MO	0–75%	48.10	4.44	8.56		5.39	7.55
EO	0–3.9%	0.39	2.08	4.12*		1.26	0.7
BA	0–2%	0.53	0.74	1.47		0.47	0.83
RBC [M μL^{-1}]	6.36–9.32	11.21	10.07	11.21		9.76	9.36
HB [g dL^{-1}]	11–15.1	18.3	16.3	18.8		15.5	15
HCT	35.1–45.4%	68.2	58.5	69.6		57.1	54.4
PLT [K μL^{-1}]	592–2972	878	888	505		574	767
MCV [fL]	45.4–60.3	60.8	58.1	62.1		58.5	58.1
MCH [pg]	14.1–19.3	16.3	16.2	16.8		15.9	16
MCHC [g dL^{-1}]	30.2–34.2	26.8	27.9	27		27.1	27.6
RDW	12.4–27%	18.6	19.7	18.2		18.3	18.7
MPV [fL]	5–20	5.4	5.5	5.7		4.9	5.1
Chemistry							
BUN [mg dL^{-1}]	2–71	38	38	24		35	33
Creat [mg dL^{-1}]	0.1–2.1	0.3	0.3	0		0.4	0.3
ALT [U L^{-1}]	7–227	114	75	296*			36
AST [U L^{-1}]	37–329	421	196	450*		92	122
ALP	13–291		151				92
GGT [U L^{-1}]	1–4		1				0
T Prot [g dL^{-1}]	3.3–7.6		6.1				
T Bili [mg dL^{-1}]	0.1–1.1		0.4				0.5

Small. Author manuscript; available in PMC 2011 August 16.

	Normal range	Control	Treated mice [mouse^{-1}]				
		0	1 mg	0.5 mg	0.25 mg	0.1 mg	0.05 mg
GLU [mg dL^{-1}]	46–279		272				
ALB [g dL^{-1}]	2.5–5.4		2.8				
Chol [mg dL^{-1}]	34–219		152				
% of Body Weight							
Liver		5.58	5.57	5.89	5.94	6.49	6.23
Spleen		0.58	0.61	0.56	0.81	0.76	0.90
Left kidney		0.81	0.89	0.62	0.69	0.99	1.12
Right kidney		0.81	0.78	0.67	0.69	0.76	1.12
Brain		2.38	2.23	2.24	2.31	2.34	2.58
Heart		0.81	0.89	0.73	0.52	1.17	1.01

[*]Value above normal range.